Comparative Techno-Economic Analysis of Parabolic Trough and Linear Fresnel Collectors with Evacuated and Non-Evacuated Receiver Tubes in Different Geographical Regions

processes

MDPI

Article

Comparative Techno-Economic Analysis of Parabolic Trough and Linear Fresnel Collectors with Evacuated and Non-Evacuated Receiver Tubes in Different Geographical Regions

Mehdi Shokrnia [1], Mattia Cagnoli [2], Roberto Grena [2], Antonio D'Angelo [3], Michela Lanchi [2,*] and Roberto Zanino [1]

[1] Dipartimento Energia, Politecnico di Torino, Corso Duca degli Abruzzi 24, 10129 Torino, Italy; mehdi.shokrnia@polito.it (M.S.); roberto.zanino@polito.it (R.Z.)
[2] ENEA, Casaccia Research Center, Via Anguillarese 301, 00123 Rome, Italy; mattia.cagnoli@enea.it (M.C.); roberto.grena@enea.it (R.G.)
[3] ENEA, Portici Research Center, Piazzale Enrico Fermi 1, 80055 Napoli, Italy; antonio.dangelo@enea.it
* Correspondence: michela.lanchi@enea.it

Abstract: In the context of Concentrated Solar Power (CSP) technology, this paper presents a comparison between the Parabolic Trough Collector (PTC) and the Linear Fresnel Collector (LFC), considering both evacuated and non-evacuated receiver tubes. The comparison was carried out in terms of the Levelized Cost of Electricity (LCOE) considering a reference year and four locations in the world, characterized by different levels of direct normal irradiation (DNI) from 2183 kWh/m^2/year to 3409 kWh/m^2/year. The LCOE depends on economic parameters and on the net energy generated by a plant on an annual basis. The latter was determined by a steady-state 1D model that solved the energy balance along the receiver axis. This model required computing the incident solar power and heat losses. While the solar power was calculated by an optical ray-tracing model, heat losses were computed by a lumped-parameter model developed along the radial direction of the tube. Since the LFC adopted a secondary concentrator, no conventional correlation was applicable for the convective heat transfer from the glass cover to the environment. Therefore, a 2D steady-state CFD model was also developed to investigate this phenomenon. The results showed that the PTC could generate a higher net annual energy compared to the LFC due to a better optical performance ensured by the parabolic solar collector. Nevertheless, the difference between the PTC and the LFC was lower in the non-evacuated tubes because of lower heat losses from the LFC receiver tube. The economic analysis revealed that the PTC with the evacuated tube also achieved the lowest LCOE, since the higher cost with respect to both the LFC system and the non-evacuated PTC was compensated by the higher net energy yield. However, the non-evacuated LFC demonstrated a slightly lower LCOE compared to the non-evacuated PTC since the lower capital cost of the non-evacuated LFC outweighed its lower net annual energy yield. Finally, a sensitivity analysis was conducted to assess the impact on the LCOE of the annual optical efficiency and of the economic parameters. This study introduces key technical parameters in LFC technology requiring improvement to achieve the level of productivity of the PTC from a techno-economic viewpoint, and consequently, to fill the gap between the two technologies.

Keywords: CSP; Parabolic Trough Collector (PTC); Linear Fresnel Collector (LFC); techno-economic analysis; numerical modelling

Citation: Shokrnia, M.; Cagnoli, M.; Grena, R.; D'Angelo, A.; Lanchi, M.; Zanino, R. Comparative Techno-Economic Analysis of Parabolic Trough and Linear Fresnel Collectors with Evacuated and Non-Evacuated Receiver Tubes in Different Geographical Regions. *Processes* **2024**, *12*, 2376. https://doi.org/10.3390/pr12112376

Academic Editor: Shumpei Funatani

Received: 14 September 2024
Revised: 21 October 2024
Accepted: 26 October 2024
Published: 29 October 2024

1. Introduction

Replacing fossil fuels with sustainable energy sources is a global challenge for the 21st century. This has drawn attention to renewable resources like solar energy [1]. Concentrated Solar Power (CSP) technology is considered an option with great potential because of its

capability to satisfy electrical and thermal energy demands as a renewable, sustainable, environmentally friendly and dispatchable form of energy [2]. The dispatchability of the energy produced depends on the integration of the solar field with a thermal energy storage system. The most commercially developed thermal energy storage technology implemented in CSP plants is the two-tank sensible storage system. In this system, cold and hot working fluids are stored in two separate tanks. However, thanks to recent advancements in energy storage technology, a single-tank thermocline storage system has been established, providing a lower investment cost. In addition, latent heat storage technology has been introduced recently to further reduce the capital costs associated with the storage system as well as the size of the storage tank [3].

The thermal energy storage in CSP systems allows for adjusting power generation based on fluctuations in demand, enhancing flexibility within the energy network. Moreover, it ensures a long-term stable power output even during low solar radiation or during the night, unlike some other renewable sources like PV and wind, which cannot provide stable power because of their absolute dependence on the environmental conditions. Furthermore, CSP systems have the advantage of the possibility of coupling with fossil fuels or other renewable energy sources [4].

Among different CSP technologies, the line-focusing systems include the Parabolic Trough Collector (PTC) and the Linear Fresnel Collector (LFC). The latter offers significant economic advantages because of its simple and low-cost design; however, the LFC suffers from a low optical efficiency compared to the PTC [5–7]. A PTC consists of parallel rows of long parabolic mirrors, while, in the LFC, the parabolic mirror is replaced by a series of nearly flat mirror stripes. Both these systems concentrate solar radiation over a focus line, where the receiver tube is located. The LFC also adopts a secondary concentrator mounted above the receiver, which allows for reconcentrating the solar radiation that misses the receiver. In the typical case of a single-tube receiver, the secondary concentrator is a Compound Parabolic Concentrator (CPC).

A receiver tube consists of a metallic absorber tube encapsulated in a glass envelope. An alternative receiver design for the LFC system is a multi-tube configuration [8,9]. The evacuated receiver tube provides the opportunity to evacuate the gap between the absorber tube and the glass, with the aim of reducing the convective heat loss and protecting the selective coating of the absorber tube from the air. However, further life cycle costs associated with an evacuated tube compared to a non-evacuated tube should be taken into account, as creating and maintaining the vacuum implies further costs. In addition, maintaining the evacuation in the gap region can be a challenge from an operational point of view since it may be lost due to unexpected accidents or physical damage to the joints. This is crucial to ensuring the minimization of convective heat losses from the receiver tube to the external environment. On the other hand, the stability of the non-evacuated coatings in air at high temperatures is still under debate. Recent studies have demonstrated important advances in the stability of these coatings at medium-high temperatures after several hours of use [10–12]. For instance, Rossi et al. [12] investigated new developed spectrally selective coatings for linear receivers operating in air at a high temperature (600 °C). These coatings confirmed their good thermal and optical stability, since only slight variations were observed in the optical properties of the coatings after over 2000 h of aging in open air conditions. Solar absorptances of 73% and 87% and thermal emissivities of 18% and 27% were reported through thermal oxidation and the sputtering process, respectively.

In the LFC, the secondary concentrator is expected to perturb the external air flow around the receiver tube, and consequently, the convective heat losses that lower the thermal efficiency of the receiver. In this regard, some studies have been conducted considering the LFC with a multi-tube receiver and a trapezoidal secondary concentrator that is closed at the bottom by a flat glass plate. Pye, Morrison and Behnia [13] investigated the unsteady flow patterns in the trapezoidal cavity of a CLFR, and they proposed a Nusselt number correlation derived from CFD simulations, which was based on the Grashof number and on the cavity depth and width. Natarajan, Reddy and Mallick [14] developed a 2D

steady-state CFD model to study combined natural convection and surface radiation heat transfer in the trapezoidal cavity absorber of a CLFR. Based on this numerical simulation, a Nusselt number correlation was proposed for the combined natural convection and surface radiation, which was a function of the Grashof number, absorber angles, surface emissivity, aspect ratio, temperature ratio and radiation-conduction number. Moving to the single-tube receiver LFC configuration, Guadamud et al. [15] studied its heat transfer in a single tube using a three-dimensional unsteady CFD model. The distribution of the Nusselt number around the azimuthal direction of the receiver tube was obtained. However, only one specific condition was considered, and no correlations were developed for the Nusselt number. Furthermore, Cagnoli et al. [16] evaluated the impact of the CPC of an LFC receiver unit on the heat losses from the absorber tube to the external ambient using 2D and 3D CFD models for the transversal and parallel wind directions as well as for natural convection. The analysis showed a slight change in the receiver performance independently of the wind direction and intensity because of the shielding effect of the CPC, but no correlations were developed for the Nusselt number. Therefore, to the best of our knowledge, no correlations to date have been established for the Nusselt number that apply to the case of the single-tube LFC receiver with a CPC secondary concentrator. Two such correlations will be derived in the present work for the cases of natural and forced convection, respectively.

To make a fair comparison among different configurations of the PTC and LFC, it was essential to perform annual optical, thermal and economic analyses. Morin et al. [5] performed a comparative analysis of a reference evacuated PTC and various configurations of the evacuated and non-evacuated LFC with CPC in terms of annual optical and thermal efficiency and electricity generation costs. As the LFC receiver tube with a 7 cm diameter represented better thermal performance in comparison with the large-diameter one (with 14 cm diameter), it was concluded that smaller receiver designs of the LFC would be more efficient. It was also proven that the LFC technology had a lower optical and thermal efficiency compared to the PTC; however, it was stated that, potentially, the lower cost per aperture area could compensate for the lower efficiency. However, they did not include all four linear technologies in their study as the non-evacuated PTC was not investigated. Furthermore, a glass plate was arranged at the bottom of the receiver unit for the LFC in their study, while a glass tube was considered in the present paper.

Cau and Cocco [17] compared the thermal performance of medium-sized (1 MWe) CSP plants comprising an Organic Rankine Cycle (ORC) unit integrated with the PTC and the LFC, using evacuated receiver tubes. The results revealed that the CSP plants based on the LFC led to higher electrical energy production per unit area of land; but, because of higher optical efficiency, the PTC provided more energy per unit area of solar collector and consequently higher conversion efficiencies. This work was then followed by Cocco and Cau [18], where an economic analysis was performed reporting that the evacuated LFC was not yet competitive with the evacuated PTC due to higher energy production cost. Nonetheless, these studies did not perform a comprehensive comparative analysis among all linear CSP technologies since they focused only on the evacuated tubes and the non-evacuated configurations were not investigated.

Sait et al. [19] optimized the performance and the cost of a Fresnel-based modular solar field through an optical and thermal analysis and compared the results with a PTC reference plant. In their study, a multi-tube receiver was considered for the LFC with eight tubes, a wedge-type secondary concentrator and a glass plate at the bottom of the receiver unit. It was reported that annual solar-to-electricity efficiency could be close to the state of the art in PTCs due to the reduction in costs thanks to lighter structures. The comparison showed that the Fresnel solar field had the potential to generate a certain level of power with approximately 2/3 of the cost of the PTC plant. However, the non-evacuated PTC and the LFC with a CPC were not included in the analysis.

Furthermore, Rovira et al. [20] compared the annual performance and the economic feasibility of integrated solar combined cycles using the PTC and the LFC and claimed that thermal contribution would be higher with the PTC, but the LFC could improve the

economic feasibility of the plant. Nevertheless, the non-evacuated configurations were not investigated in this study. Purohit and Purohit [21] evaluated the technical and economic potential of CSP systems in India and suggested the best locations across the country for CSP plants with the lowest Levelized Cost of Electricity (LCOE). The non-evacuated configurations were not considered in this assessment as well.

Some research works have also provided economic comparisons between evacuated and non-evacuated tubes. Bendato et al. [22] measured the impact of technical solutions on the economic performance indicators for three different configurations, an evacuated tube, a simply encapsulated tube and a tube with a glass plate closing the CPC unit at the bottom, by using regression meta-models built based on the theory of response surface methodology. Their results showed that, from an economic point of view, the best technological configuration would be the vacuum-sealed tube. On the contrary, the less favorable configuration was the tube in air with a glass jacket. However, only the LFC was investigated in this work. Montes et al. [23] conducted a comparative thermal and economic analysis for three single-tube receiver tubes including evacuated, non-evacuated and non-evacuated with a glass plate at the aperture. Their work studied the annual electricity cost of Fresnel plants with a hybrid loop and demonstrated that the robustness, simplicity and lower investment of the non-evacuated tubes could compensate for the higher heat loss. Nevertheless, the comparison did not involve the PTC, but only the LFC. Moreover, the thermal and economic performances of evacuated and non-evacuated PTCs were assessed by Osorio and Rivera-Alvarez [24] based on the thermal output per unit cost of the plant. It was claimed that the evacuated PTC generally provided higher thermal output per unit cost. Their work did not investigate the LFC and focused only on the PTC.

Most recently, Bellos [25] studied the potential of CSP technologies in different locations in Greece to find the most promising solution. The computed results of the LCOE for the PTC and the LFC based on the yearly DNI showed that the PTC represented a lower LCOE for different DNI values. However, the non-evacuated systems were not included in the study, and the analysis was constrained to Greek locations.

Consequently, reviewing the literature revealed the lack of a comprehensive comparative techno-economic analysis of PTC and LFC systems comprising evacuated and non-evacuated tubes. Particularly, a notable feature of this analysis is the comparison between a non-evacuated LFC and non-evacuated PTC, which is absent from the existing literature. Moreover, the application of a new selective coating (AIR PLUS) under development at ENEA, for non-evacuated tubes, might provide new insights into the economic viability of non-evacuated tubes. Furthermore, a sensitivity analysis was performed to identify key technical parameters in the LFC system that required enhancement to make this technology comparable with the PTC from a techno-economic viewpoint.

In this study, first, a mixture of molten salt (60%wt. $NaNO_3$ + 40%wt. KNO_3) working in the temperature range of 290–500 °C was considered as the HTF, and then a sensitivity analysis was performed using two diathermic (Therminol VP-1 and DelcoTerm Solar E15 (Eastman, Kingsport, Tennessee, USA)) oils working in the temperature ranges of 290–400 °C and 180–300 °C, respectively. This paper is organized as the following: In Section 2, the linear CSP systems considered in this study are described for both the PTC and LFC technologies. In Section 3, the methodology adopted to conduct this analysis is presented. Then, the ray-tracing optical model is presented, which was aimed at computing the absorbed solar heat flux (Section 4). Subsequently, the thermal model is explained in Section 5, including four subsections: the 1D model along the receiver axis to obtain net annual energy yield for each technology (Section 5.1), the lumped-parameter model in the radial direction to compute the heat losses from the receiver tube (Section 5.2), the 2D steady-state CFD model of the LFC receiver unit, which computes convective heat transfer (Section 5.3), and the corresponding results of the thermal analysis (Section 5.4). Finally, a comparison is presented among the different configurations from an economic point of view based on the LCOE, by coupling the results of the 1D model in terms of the net annual energy yield to the economic data collected from the literature (Section 6),

including a sensitivity analysis based on the parameters that affected the LCOE (Section 6.1), namely the optical efficiency (Section 6.1.1), HTF (Section 6.1.2) and economic parameters (Section 6.1.3).

2. Description of the Systems

This section describes the PTC and the LFC systems considered in this study. As a reference system for the PTC, one line of collectors with an aperture width of 5.9 m and a receiver tube with the external diameter of 0.07 m and total length of 800 m were considered, while for the LFC, 10 rows of parallel mirrors with an aperture width of 0.625 m each and a receiver tube with an external diameter of 0.07 m, a secondary concentrator of CPC type and a total length of 800 m were assumed [16,26–29]. The chosen values for the main geometric and optical parameters of the solar field are provided in Table 1 for both technologies. Figure 1 displays the scheme of the cross section of the receiver unit adopted in the LFC, including the materials for the different components. The secondary concentrator was a Compound Parabolic Concentrator (CPC). The absorber tube was made of a metallic material, encapsulated in a glass cover to reduce both convective and radiative thermal losses. The gap region between the absorber tube and the glass tube could be kept either under vacuum conditions (10^{-2} Pa), to enhance thermal insulation, or it could be simply filled with air at the atmospheric pressure. The absorber tube transferred the energy of the concentrated solar radiation to the HTF, which was molten salt (60%wt. $NaNO_3$ + 40%wt. KNO_3 [30]) in this study. In order to make the comparison between the PTC and the LFC as fair as possible, the same operating temperature of the HTF was considered (290–500 °C).

A selective coating was applied on the outer surface of the absorber tube to improve its photothermal performance. Regarding the evacuated tube, a commercially established selective coating (CERMET) was considered [31]. For the non-evacuated tube, a selective coating (AIR PLUS) under development at ENEA, which was suitable for working in air, was adopted in this study. Table 2 represents the emissivity and absorptivity of these two coatings for the evacuated and non-evacuated tubes, and Figure 2 depicts the emissivity equations.

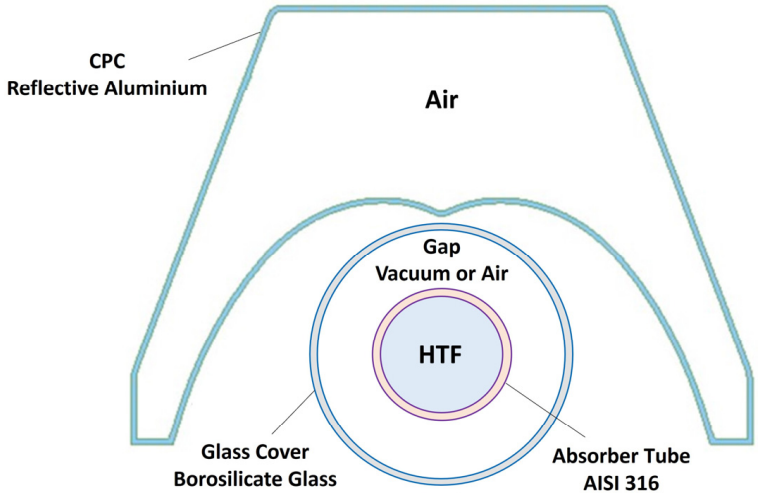

Figure 1. Scheme of the cross section of the receiver unit. This configuration was the same for both of the PTC and LFC technologies, except for the secondary concentrator, which only exists in the case of the LFC technology.

Table 1. Chosen values for the main geometric and optical parameters characterizing solar fields and receiver units.

Parameter	LFC	PTC
Number of parallel mirror lines	10	1
Collector aperture width (m)	0.625	5.9
Collector focal length (m)	4	1.81
Distance between adjacent mirrors (m)	0.825	–
Total length of the receiver tube (m)	800	800
Outer/Inner absorber tube diameter (m)	0.070/0.064	0.070/0.064
Outer/Inner glass cover diameter (m)	0.125/0.119	0.125/0.119
Primary mirrors' reflectivity	0.94	0.92
CPC reflectivity	0.90	–
Glass transmissivity	0.96	0.96
Glass refractive index	1.52	1.52
Glass extinction coefficient (m^{-1})	0.21	0.21
Receiver tube alignment	North–South	North–South

Table 2. Properties of the two coatings for the evacuated and non-evacuated tubes [31].

Configuration	Coating	Absorptivity	Emissivity
Evacuated	CERMET	0.95	$\varepsilon = 0.07513 + 2.2 \times 10^{-7} T_{abs}^2 [°C]$
Non-evacuated	AIR PLUS	0.943	$\varepsilon = 0.02339 + 1.38 \times 10^{-4} T_{abs} [°C] + 1.76 \times 10^{-7} T_{abs}^2 [°C]$

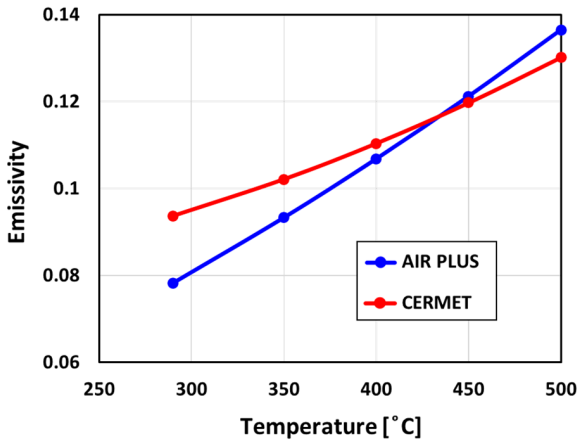

Figure 2. Emissivity as a function of the temperature for the two coatings implemented for the evacuated and non-evacuated tubes.

3. Methodology

Figure 3 summarizes the methodology implemented in this study to compare the PTC and LFC technologies from optical, thermal and economic points of view. As shown in Figure 3, firstly, an optical ray-tracing model was developed using a ray-tracing code (Tonatiuh) to compute the incident angle modifier (IAM) and the reference optical efficiency for a given PTC or LFC plant (see Section 4). This model provided the solar power incident over the receiver, which was required for the thermal analysis by the lumped-parameter and 1D thermal models. Regarding the thermal analysis, initially, a 2D CFD model was developed to estimate the convective heat losses (see Section 5.3) in the case of the LFC receiver unit. In fact, the presence of the secondary concentrator made the development of this model necessary to evaluate the convective heat transfer between the glass cover and the environment as it could be approximated by adopting correlations available in the literature (e.g., suitable for cylinders in cross flow) only in the case of the PTC. The results of the CFD model in terms of the Nusselt number were exploited by a steady-state

lumped-parameter model, developed in the radial direction by the Modelica language. The lumped-parameter model aimed at computing the heat transfer phenomena along the radial direction for a given incident solar heat flux, HTF temperature, mass flow rate, ambient temperature and (transversal) wind speed (see Section 5.2). This model calculated the heat losses from the absorber tube toward the environment for any given temperature of the HTF. The computed functions of heat losses were then exploited by the 1D thermal model, developed along the axial direction, to solve the energy balance of the heat transfer fluid, considering the hourly ambient temperature, wind speed and DNI data for the whole year (see Section 5.1). Therefore, the net annual energy yield could be calculated by the 1D model to be used in the economic analysis. To perform a comparative economic analysis based on the LCOE (see Section 6), the cost data were also required in addition to the net annual energy yield. In the present work, these cost data were collected from the literature.

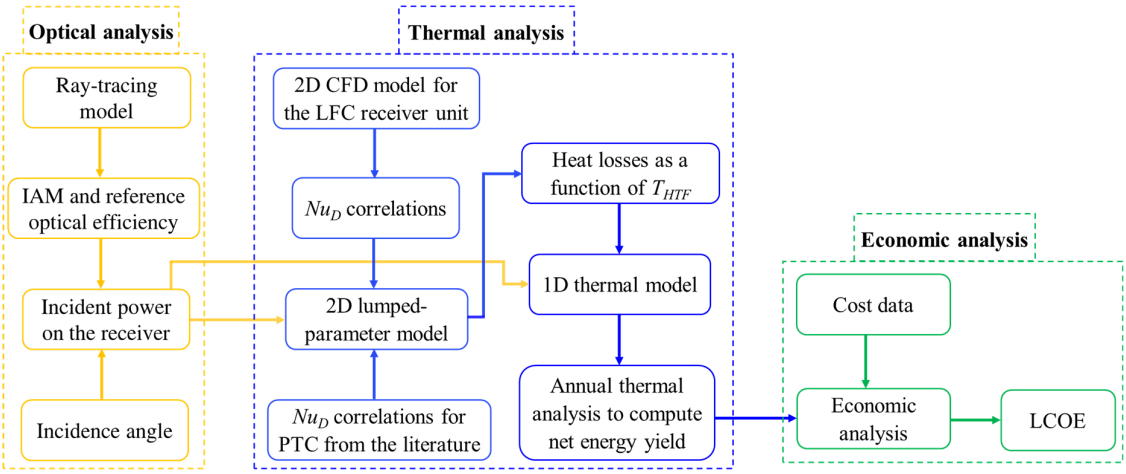

Figure 3. Global view of the methodology for the techno-economic analysis highlighting the optical analysis (Section 4), thermal analysis (Section 5) and economic analysis (Section 6).

4. Optical Analysis

This section presents the optical analysis, which was aimed at determining the thermal driver of the thermal analysis; namely, the incident power on the absorber tube per unit meter was computed as the following [17]:

$$q_{inc} = DNI \times A_c \times \eta_0 \times IAM \times \eta_{end} \times \eta_{shd} \times \eta_{cln} \quad (1)$$

where DNI is the direct normal irradiance in W/m^2, A_c is the collector aperture area in m^2, η_{end} is the end-loss efficiency, and η_{shd} and η_{cln} are the shadow efficiency and the mirror cleanliness efficiency, respectively (both assumed to be equal to 1 in this study). The term η_0 is the reference optical efficiency, i.e., the optical efficiency considering the Sun at the zenith, while the IAM is the incidence angle modifier.

The end-loss efficiency, which considers the non-irradiated receiver length at the solar field border depending on the Sun's position, is defined as the following:

$$\eta_{end} = 1 - \frac{F}{L} \times tan(\theta_l) \quad (2)$$

where F is the focal length, L is the length of the collector line and θ_l is the longitudinal incidence angle.

The IAM provides the ratio between the optical efficiency (Equation (3)) at a given incidence angle and the reference optical efficiency, at an equal DNI and aperture width. The incidence angle modifier is typically divided in the longitudinal (IAM_L) and transversal (IAM_T) components (see Equation (4)).

$$\eta = \frac{q_0}{DNI \times w} \tag{3}$$

$$IAM = IAM_T(\theta_t) \times IAM_L(\theta_l) \tag{4}$$

In Equation (3), q_0 is the absorbed solar flux per meter of collector length, given in W/m, and w is the mirror aperture width in m.

In order to determine the IAM components, as well as the reference optical efficiency, a ray-tracing model was developed using Tonatiuh [32] for both the LFC and PTC, which could compute the incident power on the absorber tube for any given Sun position. The model was based on the geometric and optical properties in Table 1, except for the collector length, which was shortened to 20 m, while the receiver was 10 m long and translated along the axial direction, depending on the Sun's position, to keep the absorber tube in the irradiated area. This allowed for the removal of any border effect, which was not taken into account in the IAM since it was considered in Equation (2). Figure 4 shows an example of the simulated solar system visualized in Tonatiuh.

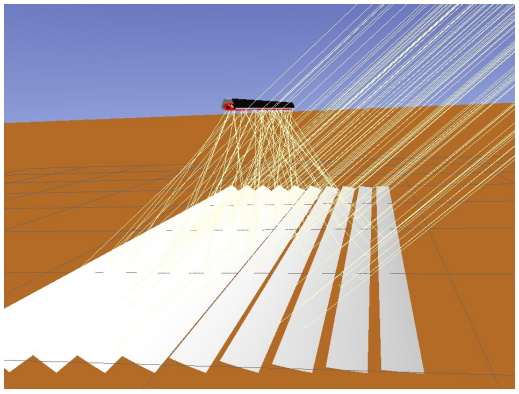

Figure 4. The solar system simulated in Tonatiuh considering the Sun in the east and the Sun's altitude being equal to 40°, with a reduced number of simulated photons for visualization purposes.

The reference optical efficiencies (Sun at zenith) computed using the ray-tracing model were equal to 0.839 and 0.878 for the LFC and the PTC, respectively. As expected, the efficiency was lower for the LFC because it only approximated a parabolic collector. A set of simulations was performed to evaluate the IAM_L and IAM_T, considering the Sun belonging to the collector longitudinal and transversal plane, respectively, and varying the Sun's altitude. Figure 5 shows the computed IAM_L and the IAM_T as a function of the incidence angle for both the technologies. For the PTC, the transversal component of the IAM was equal to 1 independently by the incidence angle, which arose from the fact that, in the PTC collector, the solar rays were always in the same plane as the normal vector to the aperture.

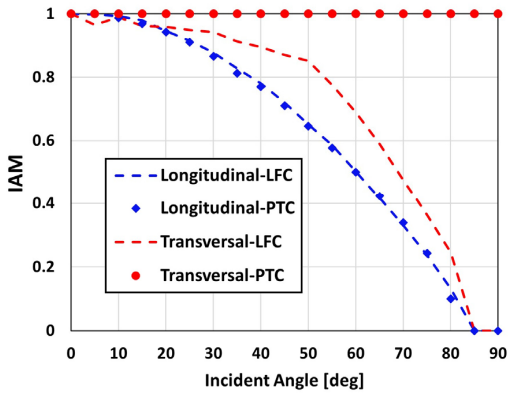

Figure 5. Incidence angle modifier components for the LFC and PTC technologies.

5. Thermal Analysis

The aim of the thermal model was to allow for the computation of the net annual energy yield for the LFC and the PTC, which was a key parameter in the economic analysis (Section 6). In this respect, a 1D model was developed to solve the energy balance of the HTF along the receiver axis (see Section 5.1). This model exploited the results of the lumped-parameter model that computed the heat losses from the absorber tube for any given HTF temperature (see Section 5.2). The lumped-parameter model was supported by a CFD model for the case of the LFC to simulate the external air flow in the presence of the secondary concentrator, determining proper correlations for the convective heat transfer coefficient (see Section 5.3). Finally, the results of the 1D thermal model in terms of the net annual energy yield are presented in Section 5.4.

5.1. D Model

To perform an economic analysis, determining the net annual energy yield was required. For this purpose, a 1D model was developed to solve the steady-state energy balance equation for the heat transfer fluid along the receiver axis direction (see Equation (5)). The steady-state assumption for this model, which was aimed at computing an annual-based scenario, was justified, since the HTF temperature profile along the tube remained consistent during the daytime due to the continuous regulation of the mass flow rate based on the DNI. The model can be defined as

$$(Q_{abs} - Q_{loss}(T))\Delta x = \dot{m}\int_{T_i}^{T_o} c_p(T)dT \quad (5)$$

where Δx is the length of the i-th control volume of the pipe given by the spatial discretization, $\dot{m}$ is the imposed mass flow rate of the HTF, c_p is the specific heat as a function of the HTF temperature, and T_i and T_o are the HTF temperatures entering and leaving the control volume, respectively. Q_{abs} and Q_{loss} are the absorbed heat flux and the heat loss toward the environment per unit length, respectively.

Figure 6 provides a schematic representation of this model. The required boundary conditions included the HTF inlet temperature and the net thermal power transferred to the fluid per unit of receiver length, which corresponded to the absorbed heat flux (computed through the incident heat flux provided by the optical model, see Section 4) net of the heat losses (provided by the lumped-parameter model, see Section 5.2). During the night, a minimum outlet temperature of 260 °C was imposed to keep the molten salt 20 °C higher than the freezing point [33], and accordingly, the minimum mass flow rate was calculated to satisfy this outlet temperature. However, during the daytime, the HTF outlet temperature could increase up to 500 °C and the mass flow rate had to be regulated based on the DNI, wind speed and ambient temperature (which was proven to be highly dependent on the DNI). In this regard, once the DNI (and consecutively absorbed heat flux) started increasing, first, the HTF outlet temperature increased to reach the maximum outlet temperature of 500 °C, and then, the mass flow rate was regulated based on the variation in the DNI. Therefore, in cases of seasonal fluctuations or transient impacts like cloud cover, which resulted in low DNI values, the HTF outlet temperature could not reach 500 °C, while the mass flow rate was considered to remain equal to the setpoint value. The mass flow control strategy based on DNI included a few steps: first, the energy balance equation (Equation (5)) was applied for the entire receiver tube as a single control volume considering the absorbed solar power, mean heat loss and the receiver inlet/outlet temperatures, which provided an initial estimate for the mass flow rate. Then, this first guess for the mass flow rate was exploited by Equation (5) with the spatial discretization of the pipe to compute the required receiver length, ensuring the desired temperature increase of the HTF (290–500 °C). The deviation between the computed length and the design receiver length (800 m) was utilized to refine the mass flow rate evaluation. This procedure was iterated by computing the new receiver length using the updated mass flow rate value and continued until the computed receiver length was equal to the design value,

indicating the accurate mass flow rate for the given DNI. Due to the appropriate initial estimate, three iterations were mostly enough to achieve the convergence in this approach. Regarding the space discretization, the receiver axis was divided in 160 control volumes of equal length, Δx, equal to 5 m. The grid independence of the results was verified.

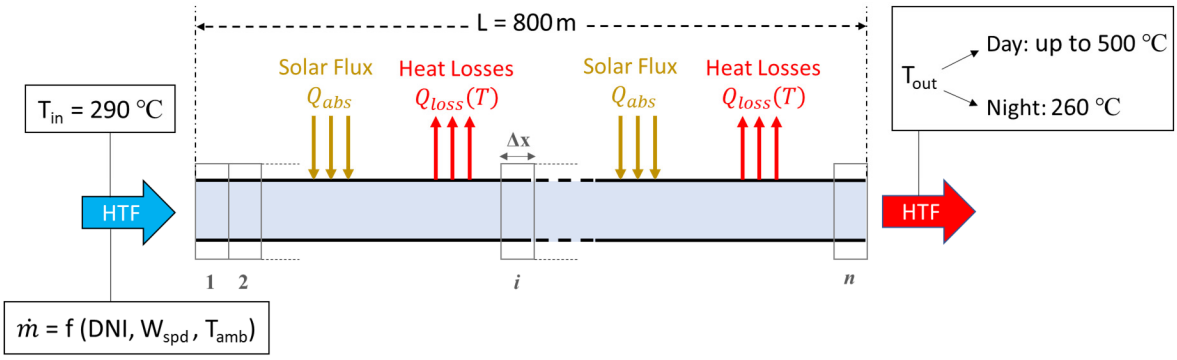

Figure 6. The scheme of the 1D model discretized along the receiver axis with the boundary conditions applied.

To compute the net energy yield, i.e., net electricity output, by the 1D thermal model, a power cycle efficiency of 38% was considered for the Rankine cycle regarding the maximum HTF outlet temperature (500 °C) in this study [34,35].

As given in Equation (5), the 1D thermal model relied on the absorbed heat flux per unit length (Q_{abs}) and the heat losses per unit length (Q_{loss}). While the former could be obtained by converting the incident power on the receiver tube given by the optical model (see Section 4), the latter had to be determined as a function of the HTF temperature through a lumped-parameter model developed in the radial direction of the receiver tube, which is represented subsequently in Section 5.2.

5.2. D Lumped-Parameter Model

This section presents the lumped-parameter model of the receiver tube cross section, which was developed using the Modelica language. This model was aimed at correlating the heat losses to the temperature of the HTF in order to determine the net power transferred to the heat transfer fluid in the 1D model (see Section 5.1). The lumped-parameter model solved the steady-state energy balance along the radial direction of the evacuated and non-evacuated receiver tube, considering the heat transfer phenomena displayed in Figure 7. The model was based on [36], with the assumptions introduced in [16], which were the following: (1) the heat loss by conduction through the support structures is negligible; (2) the glass is not fully opaque in the infrared range; and (3) the temperature of the cold sink for the heat loss by radiation, in the LFC's case, is ambient temperature, instead of sky temperature, because the CPC prevents the receiver from seeing the sky. The boundary conditions required from the model included the temperature of the HTF, the ambient temperature, the wind speed and the solar power per unit meter of receiver length incident on the absorber tube and on the glass envelope. The incident solar power came from the optical model (Section 4); the lumped-parameter model applied the absorptivity of the glass and of the selective coating applied on the absorber tube (Figure 2) to determine the share absorbed on the surface. As shown in Figure 7, the heat losses from the outer surface of the glass to the external ambient occurred by radiation and convection. The former was evaluated according to the Stefan–Boltzmann law, given the temperature of the cold sink. The convective share had to be calculated by means of Newton's law of cooling, introducing a proper heat transfer coefficient. The latter could be determined using the Churchill–Chu and Zhukauskas correlations for natural and forced convection, respectively, in the case of the PTC [37]; however, in the case of the LFC, there were no conventional correlations applicable for the convective heat transfer between the glass cover and the environment. Therefore, such correlations had to be obtained by investigating the external

air flow around the LFC receiver unit through a CFD model. The relevant correlations were established for the LFC receiver unit for natural and forced convection by a 2D steady-state CFD model, as described in Section 5.3.

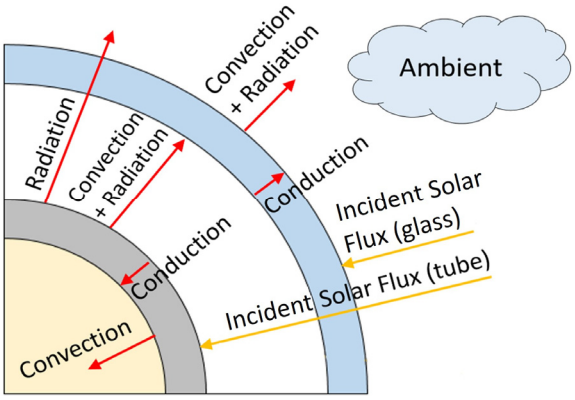

Figure 7. Heat fluxes along the radial direction considered in the lumped-parameter model, from Ref. [16].

Validation

The lumped-parameter model was validated against the experimental data provided by ENEA for the SCHOTT PTR®70 receiver tube [38]. The experiment was conducted at the ENEA Casaccia laboratory. In this test, a receiver tube with a length of about 4 m was heated by the Joule effect until it reached a practically uniform tube temperature (Figure 8). At this point, the heat loss toward the environment was measured, which was equal to the electrical power to be provided to keep the tube at the desired temperature. The inner wall temperature was measured by nine thermocouples arranged on the inner wall of the tube. As shown schematically in Figure 8, three thermocouples were located about 40 cm from the end of the tube, while the other three were located about 25 cm from the opposite end, and the last three thermocouples were located at the center of the receiver tube. The thermocouples were arranged with an angular distance of 120° among them. Both ends of the tube were closed in order to avoid air replacement inside the tube.

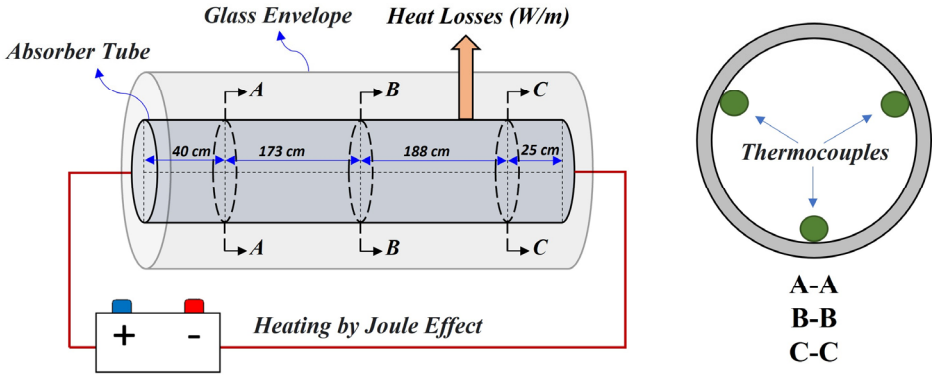

Figure 8. Experimental setup for obtaining the heat loss from the absorber tube demonstrating the schematic locations of the thermocouples.

To reproduce the experimental conditions, the model was modified. First, the thermal driver of the model was changed by replacing the solar heat flux with an imposed temperature on the absorber tube's inner wall. This implied that there was no more heat flux applied on the receiver tube and on the glass cover and that the convective heat transfer with the HTF was removed. Then, the new input data comprising coating data, tube wall temperatures and ambient temperatures were implemented. The wind speed was set to 0 (natural convection) since the test was conducted in a closed environment.

Figure 9 compares the values of the heat loss computed by the lumped-parameter model with the results of the experiment. As evident, a good agreement was obtained; i.e., the model well reproduced the experimental data, with deviation always being less than 6% and ~4% on average.

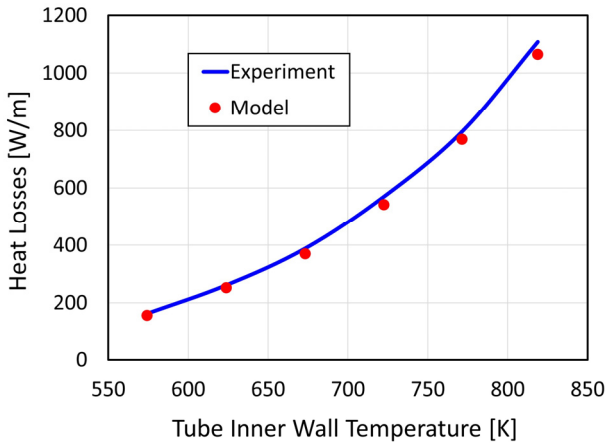

Figure 9. Comparison between the experimental data and the computed results by the lumped-parameter model for the heat loss.

5.3. CFD Model

The LFC receiver unit was investigated by means of a 2D (receiver cross section) steady-state CFD model developed using STAR-CCM+ (v. 2021.3) [39]. The CFD model was already been presented in [16]. The computational domain included the external air flow and the CPC unit; therefore, it did not include the receiver tube consisting of the absorber tube encapsulated in a glass envelope and the internal oil flow. The presence of the receiver tube was replaced by a boundary condition applied on the glass outer surface, where a uniform temperature was imposed. The latter was a valid assumption because of the slight temperature difference in the azimuthal direction within the glass envelope [16]. On the left side of the computational domain, transversal wind speed was imposed together with the (ambient) temperature of the incoming air, while on the opposite side of the domain, ambient pressure was imposed by means of a "pressure outlet" boundary condition. It can be noted that the receiver unit was not placed in the center of the external air domain, but toward the inlet section of the wind, to ensure that the vortices released downstream of the receiver unit were solved within the computational domain. In the case of no wind (pure natural convection), the ambient pressure was imposed on the top and the bottom sides of the domain, while the left and the right sides were set to be symmetrical planes. The air inside the CPC was kept at atmospheric pressure.

The computational domain was discretized, generating a mesh consisting of polygonal cells. The mesh was structured to be more refined close to the receiver unit in order to ensure the accurate solution of the velocity and thermal gradients at the near-wall regions. The mesh was also structured with different sizes in the whole domain to capture the vortices established close and downstream of the receiver. A mesh sensitivity analysis was conducted, and the minimum number of polygonal cells in the domain to achieve mesh-independent results was 1.9×10^5.

The CFD model was exploited to determine proper correlations, in terms of the Nusselt number, for the convective heat transfer between the glass and the surrounding air, considering both the cases of natural convection (absence of wind) and forced convection (wind). Once the Nusselt number (Nu_D) was determined, the convective heat transfer coefficient could be obtained by Equation (6):

$$h = \frac{k}{D} Nu_D \tag{6}$$

where k is the thermal conductivity at film temperature in W/m. k and D is the outer diameter of the tube.

In this respect, a wide parametric space was investigated, which included the wind speed, ambient temperature and glass temperature. Table 3 outlines the specified limits for these three parameters in the CFD analysis. Concerning the wind speed and ambient temperature, a reasonable range of values was considered to take into account the vast majority of the weather conditions corresponding to the meteorological data for the reference locations considered in this study. The range of the glass temperature was determined according to the HTF temperature range considered in this study (290–500 °C).

Table 3. Parametric space investigated in terms of the range of values for the parameters considered.

Parameter	Minimum Value	Maximum Value
V_w (m/s)	0	10
T_{amb} (K)	273	313
T_{glass} (K)	300	450

The results of the CFD analysis are presented in Sections 5.3.1 and 5.3.2 for natural and forced convection, respectively.

5.3.1. Natural Convection

The results of the CFD model in the absence of wind were first compared against the correlations provided by Churchill and Chu (Equation (7)) and Morgan (Equation (8)) for the case of natural convection around a long horizontal circular cylinder [37]. This comparison was performed by removing the CPC from the computational domain.

$$\overline{Nu}_D = \left\{ 0.60 + \frac{0.387\, Ra_D^{1/6}}{\left[1 + (0.559/Pr)^{9/16}\right]^{8/27}} \right\}^2 \tag{7}$$

$$\overline{Nu}_D = C\, Ra_D^n \tag{8}$$

where Ra_D represents the Rayleigh number for air based on the glass envelope's outer diameter, Pr is the Prandtl number for air at film temperature, and C and n are given in [37]. Figure 10 compares the Nusselt number computed by the present CFD model with the two correlations aforementioned, considering five different combinations of the parameters that resulted in as many values of the Rayleigh number. The obtained Rayleigh number covered the whole range in which the correlations were applicable. The Nusselt numbers computed by the CFD model agreed well with those obtained by the correlations. According to Figure 10, the maximum deviation observed in the results was 7.76%, which was quite favorable. This is because, as noted in [37], an accuracy of 20% would be acceptable for most engineering calculations in this problem.

At this point, the CPC was reintroduced in the computational domain to simulate the Fresnel case. Then, the CFD model was run again, considering the same Rayleigh numbers of the previous case. As shown in Figure 10, a significant difference could be detected between the cases with and without the CPC unit. The values were lower for the Fresnel case because of the rather low convective heat transfer around the glass envelope due to the presence of the CPC unit, which trapped the heated air moving upward because of buoyancy forces. As displayed in Figure 10, in the case of the Fresnel receiver unit, a linear equation could be found for the Nusselt number as a function of the Rayleigh number for the Fresnel case. This linear correlation (see Equation (9)) well explained the data, with the coefficient of determination (R^2) being about 0.99.

$$\overline{Nu}_D = 6.90 \times 10^{-7} Ra_D + 7.85 \tag{9}$$

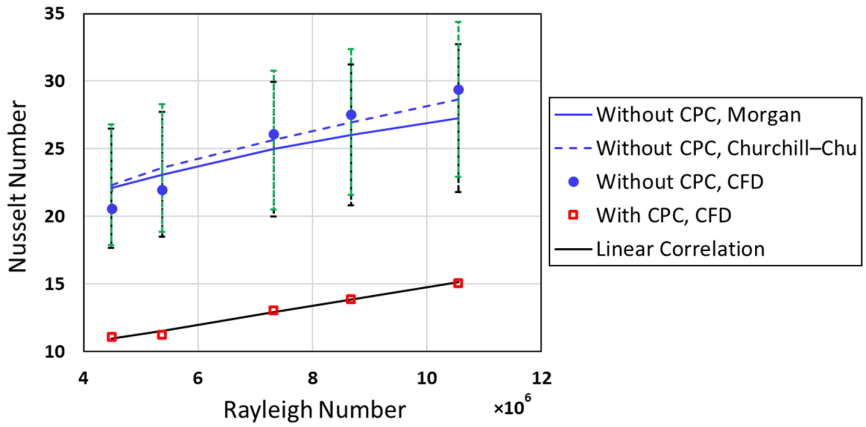

Figure 10. Comparison between the CFD model and the two correlations for natural convection around a cylinder with error bars (green dotted line for Churchill–Chu and black dotted line for Morgan) and computed Nusselt numbers for natural convection around the Fresnel collector.

5.3.2. Forced Convection

Similar to natural convection, in the case of forced convection, the model was first compared against a well-established correlation available in the literature for the case of the cylinder in cross flow, i.e., without the CPC. Particularly, the Zhukauskas correlation [37] was considered here (see Equation (10)).

$$\overline{Nu}_D = C\, Re_D^m\, Pr_a^n \left(\frac{Pr_a}{Pr_g}\right)^{1/4} \tag{10}$$

where Re_D is the Reynolds number based on the glass envelope's outer diameter, Pr_a and Pr_g are the Prandtl numbers evaluated at the atmospheric and the glass temperatures, respectively, and C, m and n are given in [37] as a function of the Re and Pr numbers.

Figure 11 compares the Nusselt numbers obtained by the CFD model and by the Zhukauskas correlation for different Reynolds numbers, which were obtained for different combinations of the parameters. The obtained range of the Reynolds number covered the entire range in which the correlation was applicable. As shown, the model reproduced the Nusselt number values predicted by the correlation well. The maximum deviation was 9.49%, which was sufficiently convincing, since the error bar for the correlations was about 20% (as shown in Figure 11), according to [37].

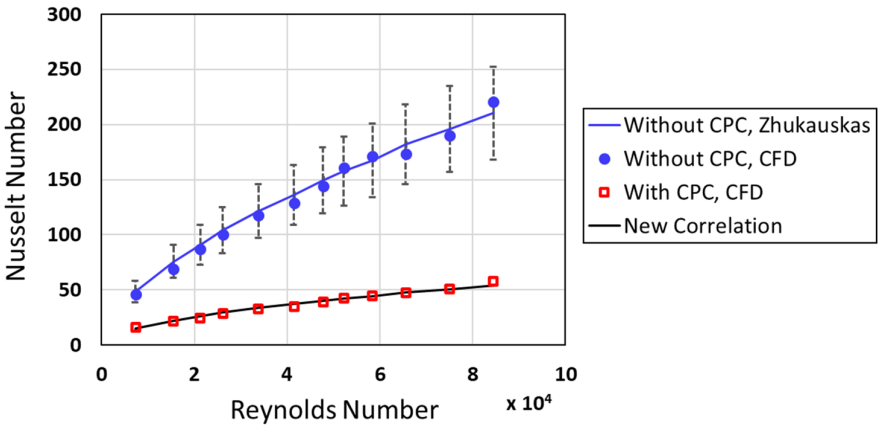

Figure 11. Comparison between the CFD model and the Zhukauskas correlation for the circular cylinder in cross flow with the error bar and computed Nusselt numbers for forced convection around the Fresnel collector.

At this point, the CPC was reintroduced in the computational domain to simulate the Fresnel case and the CFD model was run again for the same Reynolds numbers previously considered. As can be observed in Figure 11, the Nusselt number was much lower in the case with the CPC unit, which corresponded to the actual Fresnel system. This mainly arose from the lower convective heat transfer around the glass envelope due to the semi-cavity effect provided by the CPC. The magnitude of this difference was more considerable for forced convection in contrast to natural convection (Figure 10 vs. Figure 11) because of a higher air velocity magnitude, and accordingly, major variation in the heat transfer coefficient. However, in percentages, the difference was relatively comparable (~50% vs. ~70% on average in the cases of natural and forced convection, respectively).

The form of the Zhukauskas correlation (Equation (10)) was considered to develop a correlation suitable for the Fresnel case (receiver and secondary concentrator). For this purpose, the coefficients C, m and n were recalculated according to the results of the CFD model. The best interpolation of the data determined the coefficients C, m and n to be 0.165, 0.52 and 0.37, respectively (see Equation (11)).

$$\overline{Nu}_D = 0.165\ Re_D^{0.52}\ Pr_a^{0.37}\left(\frac{Pr_a}{Pr_g}\right)^{1/4} \tag{11}$$

The resulting value of the coefficient of determination (R^2) was 0.99, which represented an adequate accuracy.

5.4. Results of the Thermal Analysis

In this section, the results computed by the 1D model are presented in terms of the thermal performance for different configurations, providing an assessment of the net annual energy yield. Figure 12 shows the meteorological data comprising the DNI, wind speed and ambient temperature for a reference location (Karas, Namibia), considering a reference day with a high DNI, characterized by relatively large fluctuations (13 November). Figure 13 outlines the thermal performance of the different systems for this reference case. Early in the morning, the receiver outlet temperature started increasing (Figure 13a) following the increase in the DNI (Figure 12). However, the increase in the outlet temperature showed a delay for the case of the LFC compared to the PTC due to the difference in their optical performance as the PTC, in spite of the LFC, was not influenced by the transversal effects early in the morning when the incidence angle was higher (see Figure 5). This upsurge in the temperature was sharper for the evacuated tubes thanks to the lower heat loss compared to the non-evacuated ones (Figure 13c). In addition, the higher heat loss from the non-evacuated tubes led to the lower thermal efficiency during the daytime compared to the evacuated ones (Figure 13d). Once the HTF outlet temperature reached the desired value (500 °C), the mass flow rate started increasing from the minimum value, continuously regulated based on the DNI value (Figure 13b). The minimum required mass flow rate was higher for the non-evacuated tubes due to their higher heat loss (Figure 13c), leading to a greater temperature drop along the receiver tube during the night.

Moving to the annual-based comparison, Figure 14 shows the monthly values of the meteorological data for each of the reference locations, namely, Calama (Chile), Karas (Namibia), Leinster (Australia) and Adam (Oman), during the year (data from [40]). As shown, the location in Chile had the highest yearly solar direct beam potential with 3409 kWh/m^2, while the lowest yearly potential corresponded to the location considered in Oman, with 2183 kWh/m^2. The latitudes of the aforementioned locations were the following: Calama (Chile) was located at 22.49° S, Karas (Namibia) at 25.63° S, Leinster (Australia) at 27.79° S and Adam (Oman) at 22.51° N. For each location, hourly meteorological data comprising the DNI, wind speed and ambient temperature were considered to calculate the annual energy yield by means of the 1D model.

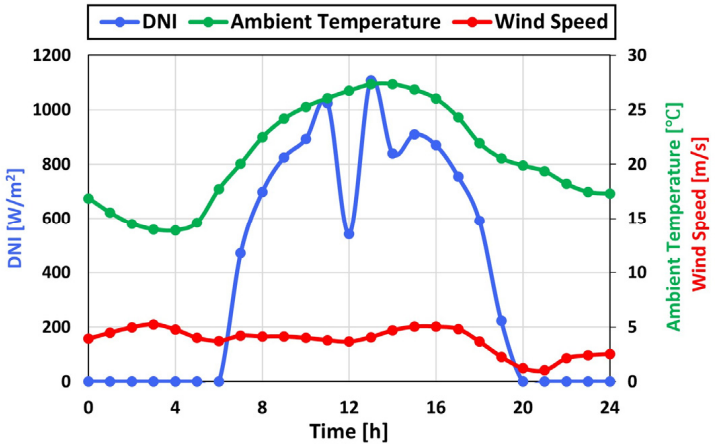

Figure 12. Meteorological data including the DNI, wind speed and ambient temperature for the reference location (Karas, Namibia) and the reference day (13 November).

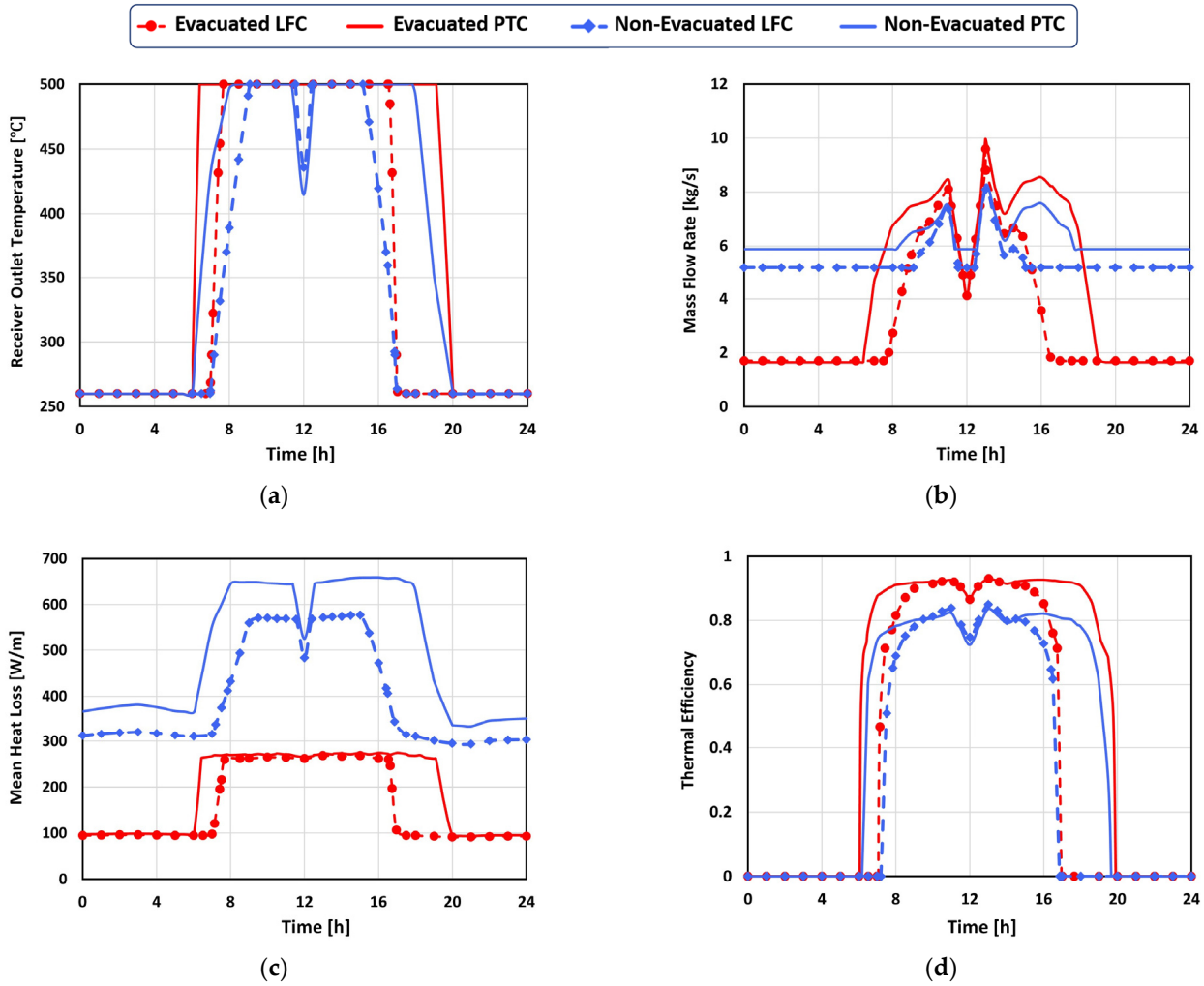

Figure 13. Thermal performance of the different configurations considering the reference day (13 November) in terms of the (**a**) receiver outlet temperature, (**b**) mass flow rate, (**c**) mean heat loss and (**d**) thermal efficiency.

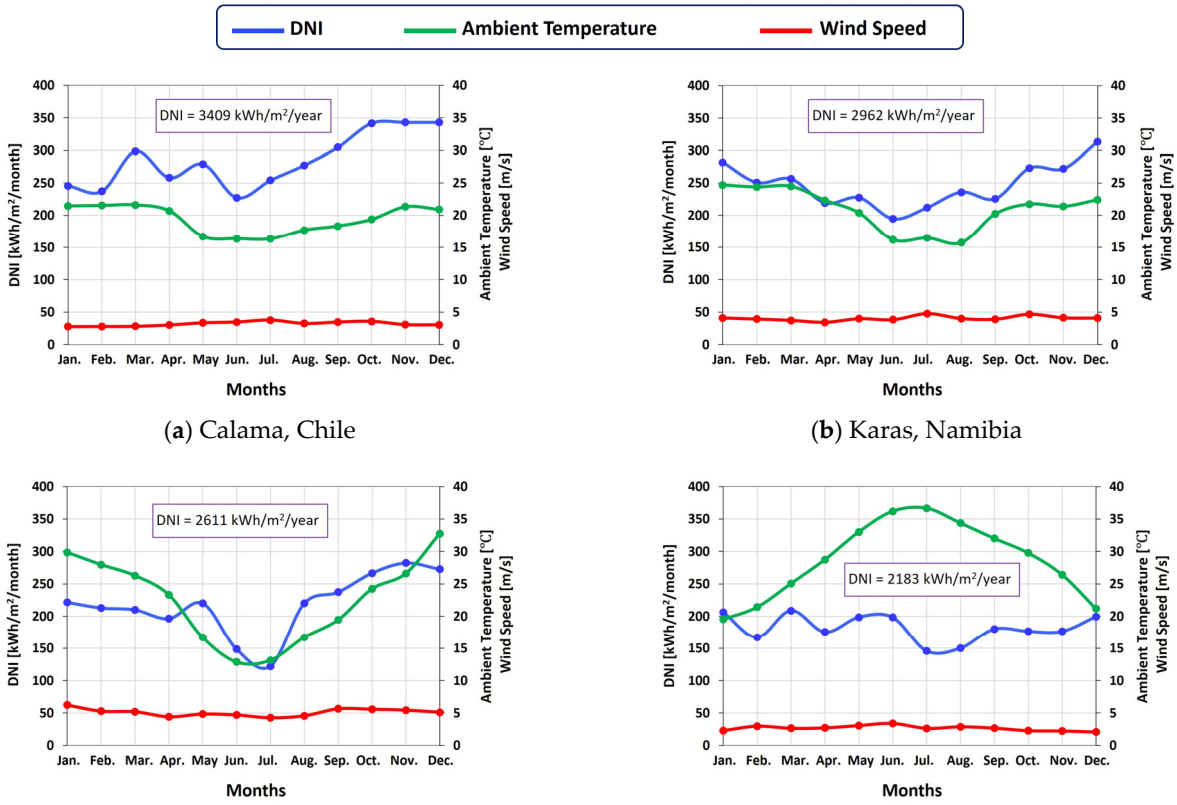

(**a**) Calama, Chile

(**b**) Karas, Namibia

(**c**) Leinster, Australia

(**d**) Adam, Oman

Figure 14. Reference meteorological data including DNI, wind speed and ambient temperature for the different locations under investigation.

Figure 15 displays the net monthly energy yield during the year calculated for the reference locations considering different configurations. Considering the N–S alignment of the receiver tube, during the summer, the collectors are exposed to extended duration of the sunlight with a high transversal angle early in the morning and late in the afternoon. Consequently, the optical performance of the LFC is dramatically influenced in this period, despite the PTC that remains unaffected by this factor (see Figure 5). As a result, the PTC performance is much more efficient at the beginning/end of the year for the locations in the southern hemisphere, as shown in Figure 15. However, for the location in Oman, closer to the equator, smaller variations in daytime duration throughout the year results in a more balanced ratios of PTC/LFC in terms of the net monthly energy yield. Moving to the comparison of the evacuated and non-evacuated tubes for each individual technology (PTC or LFC), identical patterns of variations can be observed throughout the year for both configurations, regardless of the location. This is because the difference in the thermal performance remains almost constant owing to the same patterns of wind speed throughout the year (see Figure 14).

Figure 16 outlines the net annual energy yields for the reference locations and for the different configurations. As expected, the evacuated tube allowed for a higher net energy yield to be reached compared to the non-evacuated tube because of the higher thermal efficiency for the evacuated case. This higher efficiency was due to the lower heat losses ensured by the evacuation. This result applied to both the PTC and LFC technologies, independent of the location. The PTC generated higher energy in both evacuated and non-evacuated cases thanks to the better optical efficiency in comparison with the LFC. In fact, the parabolic shape of the PTC resulted in a more efficient optical design by focusing sunlight more effectively onto the receiver tube, compared to linear mirrors of the LFC. However, the benefit of the PTC with respect to the LFC was lower than the performance improvement obtainable using an evacuated tube instead of a non-evacuated

one. Moreover, the contrast in the net annual energy yield generated by the PTC and by the LFC was less noticeable when considering the non-evacuated tubes in comparison with the evacuated tubes for each location. This is because the LFC receiver tube was protected against the wind by the secondary concentrator; thus, it was less sensible to convective heat losses, which instead strongly penalized the PTC without the thermal insulation provided by the vacuum. Comparing different locations revealed that the ratio of the net annual energy yield generated by the non-evacuated tube to that generated by the evacuated tube remained unaffected by the location (approximately 0.72 for the PTC). In fact, due to the relatively identical wind speed for all the locations throughout the year (Figure 14), the difference between the two configurations in terms of the thermal performance was not influenced by the location. Similarly, the ratio of LFC/PTC in terms of the net annual energy yield remained almost unchanged across the locations (approximately 0.86) due to the absence of variation in the proportional optical performance. In addition, the net annual energy yield followed the trend of the available yearly DNI (Figure 14), as expected.

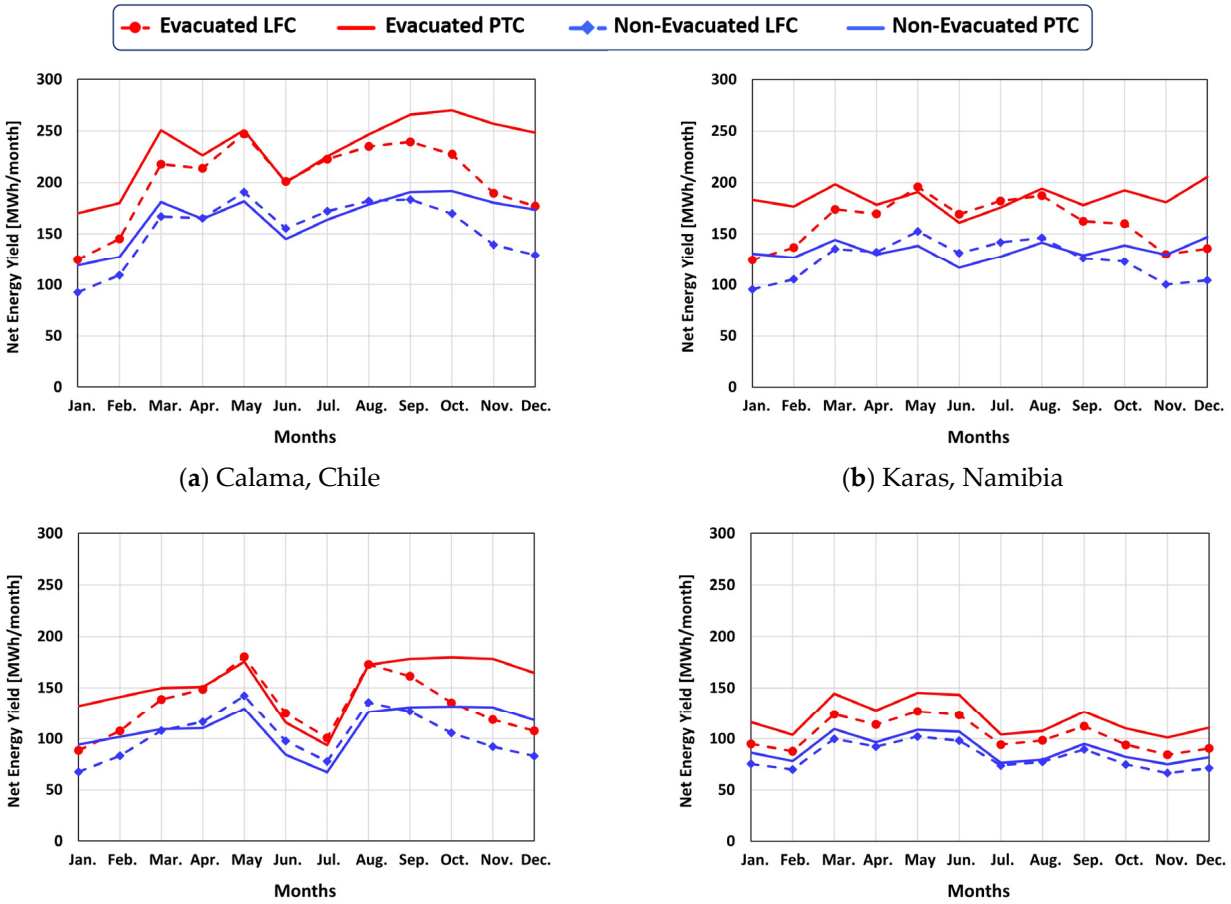

(**a**) Calama, Chile

(**b**) Karas, Namibia

(**c**) Leinster, Australia

(**d**) Adam, Oman

Figure 15. Net monthly energy yields for the reference locations during the year considering the different configurations.

The results obtained in the thermal analysis of various linear CSP systems could have significant implications for real-world CSP installations. For instance, it was noticed that, independent of the location in the northern/southern hemisphere and the latitude, the ratio of LFC/PTC in terms of the net annual energy yield consistently increased with an increase in the DNI. In fact, a higher yearly solar irradiance generally implied higher peak DNI values during midday throughout the year, when the optical performance of the LFC tended to be significantly higher compared to early morning and late afternoon. Nevertheless, the impact of this trend on the PTC was less substantial. Furthermore, no

major variation was observed in the ratio of the net annual energy yield generated by the non-evacuated tube to that generated by the evacuated tube for various locations. This is because of the relatively identical wind speed for all the locations throughout the year. In addition, the dispatchability of CSP plants could be further enhanced by the integration of thermal energy storage systems. According to the results of the thermal analysis, it can be concluded that the evacuated PTC would provide better compatibility with a storage system among all technologies under investigation since it ensures a reduced demand for auxiliary power production.

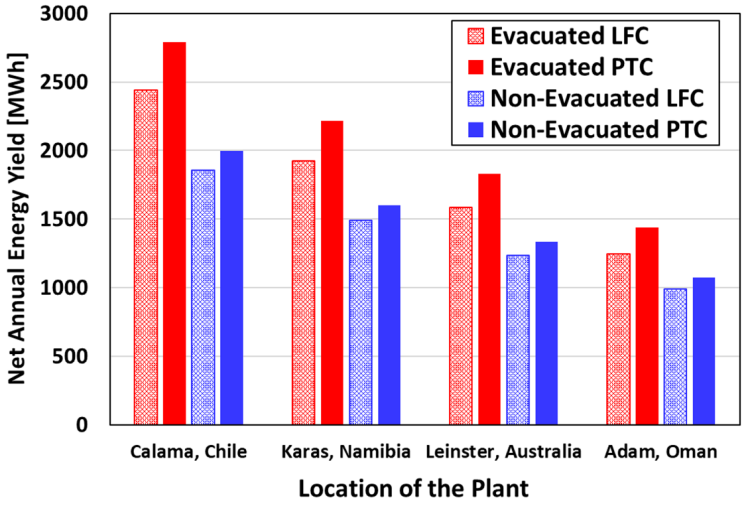

Figure 16. The net annual energy yields for the reference locations considering different configurations.

6. Economic Analysis

To properly compare the different linear systems (PTC and LFC) by adopting different receiver technologies (evacuated and non-evacuated), an analysis was carried out to exploit the results of the thermal analysis, i.e., the net annual energy yield. This economic analysis was based on the data reported in Table 4. Although economic parameters may have varied for the different locations in terms of labor costs, land costs, etc., or encountered challenges in terms of governmental regulations and incentives, assuming the same cost of data across the locations was still reasonable. Firstly, a huge proportion of the capital costs, including the costs of equipment provided by global suppliers, would not have varied with location. Secondly, a sensitivity analysis was conducted in Section 6.1, taking into account the variability in the cost data among the locations.

Table 4. Assumed cost data for the present economic analysis of the linear CSP plants.

Parameter	Value	Reference
PTC solar field (EUR/m^2)	161 *	[24,41]
LFC solar field (EUR/m^2)	138 *	[42,43]
Evacuation of the tube (EUR/m)	32	[22]
Site improvement (EUR/m^2)	18 *	[42,43]
HTF system (EUR/m^2)	43 *	[42,43]
Power block (EUR/kW_e)	1010 *	[42,43]
TES system (EUR/kWh_t)	29 *	[42,43]
Contingency (% of direct cost)	7	[23,44,45]
EPC and owner cost (% of direct cost)	10	[23,44,46]
Discount rate	0.1	[47–49]
Useful life of the plant (years)	30	[47–49]
Annual cost of operation and maintenance (% of CAPEX)	2	[47–49]

* Currency conversion (30 August 2023): EUR 1.00 ↔ USD 1.09.

This economic comparison was based on the Levelized Cost of Electricity (LCOE) in EUR/MWh, which is a key parameter in the financial evaluation of power plants because it represents a standardized criterion for evaluating the long-term economic viability of power plants, taking into account the initial investment, operational cost, discount rate, lifetime of the power plant and net annual electricity output. The LCOE is defined as the following [47,48]:

$$\mathrm{LCOE} = \frac{\mathrm{CAPEX} \times \left(\frac{\mathrm{d}(1+\mathrm{d})^{\mathrm{n}}}{(1+\mathrm{d})^{\mathrm{n}}-1} \right) + \mathrm{OPEX}}{\mathrm{NAEO}} \quad (12)$$

where CAPEX is the capital expenditure of the plant, d is the discount rate, n is the useful life of the plant, OPEX is the annual cost of operation and maintenance, and NAEO is the net annual electricity output (energy yield) provided by the plant in MWh. In order to calculate the LCOE by using Equation (12) for different configurations, the NAEO was obtained by the thermal model (Section 5.4), and the other parameters are given in Table 4.

Figure 17 shows the LCOE computed for the reference locations considering the different configurations. It should be noted that, although the economic data did not change with the location, the economic portion in the LCOE correlation (Equation (12)) varied proportionally to the net energy yield across the locations in terms of power block cost and TES system cost. Considering the evacuated tubes, Figure 17 indicates that the PTC was more economical compared to the LFC because the higher capital cost (see Table 4) was compensated by the higher optical efficiency, which led to a higher net energy yield (see Figure 16). This result also depended on the fact that the LFC technology is less mature than the PTC and there is still space for relevant improvements [50]. Moving to the non-evacuated tubes, the scenario was different, since the LFC allowed for reaching a slightly lower LCOE compared to the PTC, which meant that the lower capital cost of the non-evacuated LFC outweighed its lower net annual energy yield. This is because the difference between the net annual energy yield provided by the PTC and by the LFC was lower in the case of the non-evacuated tubes compared to the evacuated ones for each location (as discussed in Figure 16). In addition, it was evident from Figure 17 that the evacuated tubes showed lower a LCOE compared to the non-evacuated tubes for the different locations in spite of the higher cost of the evacuation of the receiver tube. This is due to the fact that the increase in the thermal efficiency, and consequently, in the net annual energy yield provided by the vacuum outweighed the higher capital cost required for evacuating the tube. In other words, the enhancement in the thermal performance due to the thermal insulation provided by the vacuum justified the cost of the evacuation.

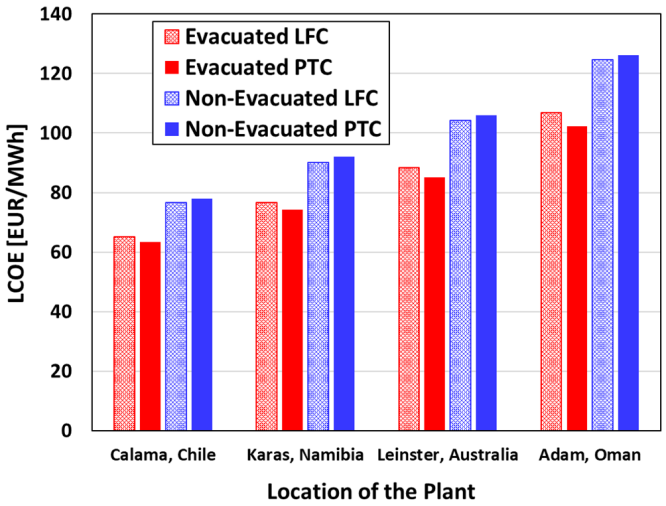

Figure 17. The LCOEs for the reference locations considering different configurations.

6.1. Sensitivity Analysis

To investigate the impact of different parameters on the LCOE, performing a sensitivity analysis was essential. Moreover, since the cost data could be variable for different locations considered in this study, the sensitivity analysis could take into account the cost variations among the locations. In this section, a sensitivity study was conducted based on the parameters that affected the LCOE (Equation (12)), namely the optical efficiency (and corresponding net energy yield), solar field HTF, CAPEX, OPEX and discount rate. The reference location for this study was that in Namibia with a DNI of 2962 kWh/m^2/year (see Figure 14b).

6.1.1. Optical Efficiency

Starting with the optical efficiency, the annual average values, based on the results of Section 6, were 61% and 47%, corresponding to the net annual energy yields of 2235 MWh and 1926 MWh for the PTC and the LFC, respectively. The relevant difference in the optical efficiency was the main reason for the lower energy yield of the LFC compared to the PTC. In this regard, a sensitivity analysis was performed by varying the annual optical efficiency of the LFC, and accordingly the net annual energy yield, to assess the impact of variations in the LCOE. This study was performed through an analytical approach aimed at determining the minimum value of the annual optical efficiency for the LFC that would lead to the same LCOE of the PTC. This analysis demonstrated that an increase of approximately 6% in the annual optical efficiency of the LFC would lead to an increase of 245 MWh in the net annual energy yield. This variation corresponds to a reduction of over EUR 3/MWh in the LCOE of the LFC, which would make it as economical as the PTC, assuming that this improvement in the optical performance could be achieved without further increasing the capital cost of the plant. Such an improvement could be feasible as proven by Ref. [51], in which an optimized LFC system could reach an annual optical efficiency of over 60%, increased by 13% compared to the original non-optimized LFC system. Nevertheless, the potential economic consequences of this optimization have not been investigated.

6.1.2. HTF

As mentioned in Section 2, molten salt was considered as the HTF in this study with an operational temperatures of 290–500 °C. However, linear CSP systems may operate at lower temperatures as well. By reducing operating temperatures, the thermal insulation provided by an evacuated tube should impact thermal efficiency progressively less; in fact, heat losses depend on the temperature of the HTF. Therefore, the non-evacuated tube technology may have had a better LCOE than the evacuated tube case for sufficiently low temperatures. In this respect, a sensitivity analysis based on the HTF temperature was performed to identify the impact of this parameter on the LCOE. Hence, the reference plant with molten salt was compared with two other cases: a medium-temperature plant with thermal oil (Therminol VP-1) as the HTF operating at the temperatures of 290–400 °C and a low-temperature plant with thermal oil (DelcoTerm Solar E15) as the HTF operating at the temperatures of 180–300 °C. The power cycle efficiencies for the Rankine cycle were considered to be 35% and 31% for the medium-temperature and low-temperature plants, respectively [34,35].

Figure 18 shows the LCOE variations using different HTFs at low, medium and high temperatures. As expected, using molten salt as a high-temperature HTF led to a drop in the LCOE because of the increase in the electricity production provided by the higher temperature. However, the non-evacuated LFC indicated a bigger drop in the LCOE with an increase in the HTF temperature compared to the non-evacuated PTC, which demonstrated a relatively greater advantage of the LFC at higher temperatures. This fact implies that the percentage of the increase in the net energy yield with the increase in the HTF temperature was slightly greater for the LFC compared to the PTC. This is in agreement with the annual thermal efficiencies where, corresponding to the increase in heat losses due to an increase in the HTF temperature, the LFC encountered a relatively lower drop in the thermal efficiency

compared to the PTC, due to the benefit of its secondary concentrator. Nevertheless, in the case of the evacuated tubes, a more considerable drop could be seen in the LCOE at higher temperatures compared to the non-evacuated cases. While the LCOE of the evacuated PTC accounted for nearly 86% of that of the non-evacuated PTC at low temperature, it dropped to 80.7% in the case of the high HTF temperature.

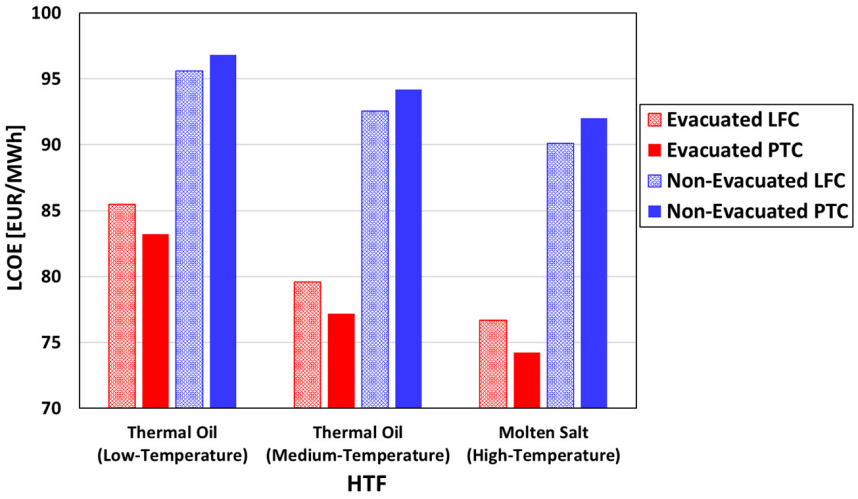

Figure 18. LCOE variation using different HTFs operating at low, medium and high temperatures for various configurations.

6.1.3. Capital Cost

Moreover, since the capital cost plays a crucial role in the LCOE, a sensitivity analysis was conducted to determine the impact of the capital cost on equalizing the LCOE for the evacuated LFC and the evacuated PTC. In this regard, the capital cost of the PTC was kept constant, while the capital cost of the LFC was varied. According to Figure 19, a reduction of over 4% in the capital cost of the evacuated LFC would make it possible to achieve the same LCOE of the evacuated PTC. However, such a reduction in the capital cost of the LFC should be achieved based on equal performances of the plant.

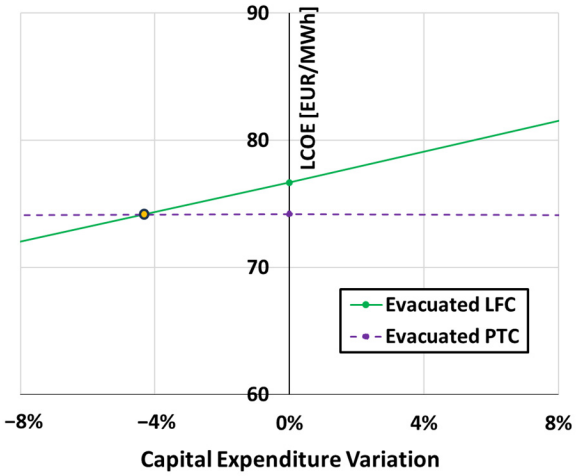

Figure 19. Sensitivity analysis representing the impact of the capital cost on equalizing the LCOE for the LFC and the PTC.

7. Conclusions and Perspective

This work compared different line-focusing systems (PTC and LFC) and different receiver technologies (evacuated and non-evacuated tubes) from optical, thermal and economic viewpoints. For this purpose, a 1D receiver model was developed along a collector axis evaluating the net annual energy yield, considering hourly meteorological

data for the entire year to be exploited in the economic analysis for each configuration. The 1D receiver model was supported by two models: an optical ray-tracing model and a lumped-parameter model.

In the case of the LFC system, the presence of its secondary concentrator strongly affected the external air flow surrounding the receiver, which made the common correlations for cylinders in cross flow not applicable here. For this reason, the development of a 2D steady-state CFD model was necessary to simulate the convective heat transfer occurring between the glass envelope and the environment, considering the presence of a secondary concentrator (CPC) for different glass temperatures, wind speeds and ambient temperatures. The results of this analysis allowed for the generation of proper correlations for the convective heat losses in the case of the LFC system. The CFD analysis proved that the heat lost by convection in the case of the LFC receiver unit was much lower in comparison with the case of the PTC, which could be properly described by correlations suitable for cylinders in cross flow. This is because the CPC unit actually protected the receiver against the wind, exhibiting a semi-cavity effect. In the absence of wind (natural convection), the CPC unit still allowed for the reduction in convective heat losses since it trapped the heated air that moved upward, reducing the replacement of the hot air with fresh air at ambient temperature.

The thermal performance of the different configurations was investigated using a 1D receiver model considering four reference locations with DNIs varying from 2183 kWh/m^2/year to 3409 kWh/m^2/year. The results showed that the PTC could generally generate a higher net annual energy yield than the LFC, both with evacuated and non-evacuated tubes, due to the better optical performance provided by the parabolic solar collector. However, the difference between the net energy yield provided by the PTC and by the LFC was lower in the case of the non-evacuated tube, owing to lower heat losses from the LFC receiver tube.

Subsequently, an economic analysis was performed based on the LCOE, exploiting the net annual energy yield computed for each location by the thermal model and considering the cost data collected from the literature. It was found that the PTC system led to a lower LCOE in the case of the evacuated tubes, with the lowest LCOE of EUR 63.4/MWh for the highest DNI location (in Chile), as the higher capital cost of the evacuated PTC was compensated by the higher optical efficiency, which is in agreement with the previous findings available in the literature. However, the non-evacuated LFC represented a slightly lower LCOE compared to the non-evacuated PTC for various locations, since the lower capital cost of the non-evacuated LFC outweighed its lower net annual energy yield. Additionally, the evacuated tubes demonstrated lower LCOEs compared to the non-evacuated tubes.

Moving to the comparison of the locations with regard to each individual configuration, the lowest and the highest LCOEs were found for the locations considered in Chile and in Oman, respectively, following the trend of the net annual energy yield. Finally, a sensitivity analysis was performed based on the key parameters involved in the LCOE, including the optical efficiency (and corresponding net energy yield), solar field HTF, CAPEX, OPEX and discount rate. It was found that an increase of approximately 6% in the annual optical efficiency of the LFC would result in an increase of 245 MWh in the net annual energy yield, corresponding to a reduction of over EUR 3/MWh in the LCOE. Such an improvement in the LFC would make it as economical as the PTC, assuming no further increase in the capital cost. The sensitivity analysis using three different HTFs at low, medium and high temperatures demonstrated a more considerable upsurge in the LCOE for the evacuated tubes at lower temperatures compared to the non-evacuated cases. Furthermore, the variability in the economic parameters was investigated through a sensitivity analysis on the input cost data, and this revealed that a reduction of nearly 4% in the capital cost of the evacuated LFC would make it possible to achieve the same LCOE of the evacuated PTC. These improvements require advancements in its mirror design, more accurate tracking mechanisms or any structural innovations in the LFC technology. It should be noted that, although some uncertainties were addressed to some extent by including crucial parameters

in terms of the contingency, EPC and owner cost in this analysis, specific challenges related to governmental regulations and incentives may still vary among different countries.

In perspective, the present work could be the starting point of further investigations. The CFD model developed in the present work could be validated experimentally by considering the LFC receiver unit investigated in this study. In addition, more optimized LFC designs could be established to make it more competitive with PTC technology. Furthermore, a techno-economic analysis could be carried out considering more enhanced selective coatings for non-evacuated tubes

Author Contributions: Conceptualization, M.C. and M.L.; data curation, R.G. and A.D.; formal analysis, M.S. and M.C.; funding acquisition, M.L. and R.Z.; investigation, M.S. and M.C.; methodology, M.S. and M.C.; project administration, M.L. and R.Z.; resources, A.D. and M.L.; software, M.S., M.C. and R.G.; supervision, M.L. and R.Z.; validation, M.S., M.C. and R.G.; writing—original draft, M.S.; writing—review and editing, M.C., R.G., A.D., M.L. and R.Z. All authors have read and agreed to the published version of the manuscript.

Funding: This research was funded by the Italian Ministry of Environment and Energy Security through the "National Electric System Research" Programme, Project 1.9 "CSP/CST technology" 2022–2024 implementation plan.

Data Availability Statement: The raw data supporting the conclusions of this article will be made available by the authors on request.

Conflicts of Interest: The authors declare no conflicts of interest.

References

1. Pavlović, T.M.; Radonjić, I.S.; Milosavljević, D.D.; Pantić, L.S. A Review of Concentrating Solar Power Plants in the World and Their Potential Use in Serbia. *Renew. Sustain. Energy Rev.* **2012**, *16*, 3891–3902. [CrossRef]
2. Jiang, K.; Du, X.; Kong, Y.; Xu, C.; Ju, X. A Comprehensive Review on Solid Particle Receivers of Concentrated Solar Power. *Renew. Sustain. Energy Rev.* **2019**, *116*, 109463. [CrossRef]
3. Shokrnia, M.; Cagnoli, M.; Gaggioli, W.; Liberatore, R.; Russo, V.; Zanino, R. Geometrical and PCM Optimization of a Thermocline Energy Storage System. *J. Energy Storage* **2024**, *98*, 113070. [CrossRef]
4. Fuqiang, W.; Ziming, C.; Jianyu, T.; Yuan, Y.; Yong, S.; Linhua, L. Progress in Concentrated Solar Power Technology with Parabolic Trough Collector System: A Comprehensive Review. *Renew. Sustain. Energy Rev.* **2017**, *79*, 1314–1328. [CrossRef]
5. Morin, G.; Dersch, J.; Platzer, W.; Eck, M.; Häberle, A. Comparison of Linear Fresnel and Parabolic Trough Collector Power Plants. *Sol. Energy* **2012**, *86*, 1–12. [CrossRef]
6. Richter, C. *Solar Power and Chemical Energy Systems*; SolarPACES Annual Report; International Energy Agency (IEA): Paris, France, 2008.
7. Giostri, A.; Binotti, M.; Silva, P.; Macchi, E.; Manzolini, G. Comparison of Two Linear Collectors in Solar Thermal Plants: Parabolic Trough Versus Fresnel. *ASME J. Sol. Energy Eng.* **2012**, *135*, 011001. [CrossRef]
8. Montes, M.J.; Abbas, R.; Barbero, R.; Rovira, A. A New Design of Multi-Tube Receiver for Fresnel Technology to Increase the Thermal Performance. *Appl. Therm. Eng.* **2022**, *204*, 117970. [CrossRef]
9. Altmann, F.; Cheng, A.S. Evaluation of a Prototype Integrated Solar Combined-Cycle Power Plant Using a Linear Fresnel Reflector. In Proceedings of the ASME 2017 11th International Conference on Energy Sustainability, Charlotte, NC, USA, 26–30 June 2017.
10. Wang, X.; Lee, E.; Xu, C.; Liu, J. High-Efficiency, Air-Stable Manganese–Iron Oxide Nanoparticle-Pigmented Solar Selective Absorber Coatings Toward concentrating Solar Power Systems Operating at 750 °C. *Mater. Today Energy* **2021**, *19*, 100609. [CrossRef]
11. Raccurt, O.; Disdier, A.; Bourdon, D.; Donnola, S.; Stollo, A.; Gioconia, A. Study of the Stability of a Selective Solar Absorber Coating under Air and High Temperature Conditions. *Energy Procedia* **2015**, *69*, 1551–1557. [CrossRef]
12. Rossi, G.; D'Angelo, A.; Diletto, C.; Esposito, S.; Guglielmo, A.; Lanchi, M. New Spectrally Selective Coatings for Csp Linear Receivers Operating in Air at High Temperature. *Appl. Res.* **2024**, *3*, e202200117. [CrossRef]
13. Pye, J.; Morrison, G.; Behnia, M. Transient Modelling of Cavity Receiver Heat Transfer for the Compact Linear Fresnel Reflector. In Proceedings of the ANZSES 2003 Destination Renewables Conference, Melbourne, Australia, 26–29 November 2003.
14. Natarajan, S.K.; Reddy, K.S.; Mallick, T.K. Heat Loss Characteristics of Trapezoidal Cavity Receiver for Solar Linear Concentrating System. *Appl. Energy* **2012**, *93*, 523–531. [CrossRef]
15. Guadamud, E.; Oliva, A.; Lehmkuhl, O.; Rodriguez, I.; González, I. Thermal Analysis of a Receiver for Linear Fresnel Reflectors. *Energy Procedia* **2015**, *69*, 405–414. [CrossRef]
16. Cagnoli, M.; Mazzei, D.; Procopio, M.; Russo, V.; Savoldi, L.; Zanino, R. Analysis of the Performance of Linear Fresnel Collectors: Encapsulated Vs. Evacuated Tubes. *Sol. Energy* **2018**, *164*, 119–138. [CrossRef]
17. Cau, G.; Cocco, D. Comparison of Medium-Size Concentrating Solar Power Plants Based on Parabolic Trough and Linear Fresnel Collectors. *Energy Procedia* **2014**, *45*, 101–110. [CrossRef]

18. Cocco, D.; Cau, G. Energy and Economic Analysis of Concentrating Solar Power Plants Based on Parabolic Trough and Linear Fresnel Collectors. *Proc. Inst. Mech. Eng. Part A: J. Power Energy* **2015**, *229*, 677–688. [CrossRef]
19. Sait, H.H.; Martinez-Val, J.M.; Abbas, R.; Munoz-Anton, J. Fresnel-Based Modular Solar Fields for Performance/Cost Optimization in Solar Thermal Power Plants: A Comparison with Parabolic Trough Collectors. *Appl. Energy* **2015**, *141*, 175–189. [CrossRef]
20. Rovira, A.; Barbero, R.; Montes, M.J.; Abbas, R.; Varela, F. Analysis and Comparison of Integrated Solar Combined Cycles Using Parabolic Troughs and Linear Fresnel Reflectors as Concentrating Systems. *Appl. Energy* **2016**, *162*, 990–1000. [CrossRef]
21. Purohit, I.; Purohit, P. Technical and Economic Potential of Concentrating Solar Thermal Power Generation in India. *Renew. Sustain. Energy Rev.* **2017**, *78*, 648–667. [CrossRef]
22. Bendato, I.; Cassettari, L.; Mosca, M.; Mosca, R. Stochastic Techno-Economic Assessment Based on Monte Carlo Simulation and the Response Surface Methodology: The Case of an Innovative Linear Fresnel Csp (Concentrated Solar Power) System. *Energy* **2016**, *101*, 309–324. [CrossRef]
23. Montes, M.J.; Abbas, R.; Muñoz, M.; Muñoz-Antón, J.; Martínez-Val, J.M. Advances in the Linear Fresnel Single-Tube Receivers: Hybrid Loops with Non-Evacuated and Evacuated Receivers. *Energy Convers. Manag.* **2017**, *149*, 318–333. [CrossRef]
24. Osorio, J.D.; Rivera-Alvarez, A. Influence of the Concentration Ratio on the Thermal and Economic Performance of Parabolic Trough Collectors. *Renew. Energy* **2022**, *181*, 786–802. [CrossRef]
25. Bellos, E. A Geospatial Comparative Analysis of Solar Thermal Concentrating Power Systems in Greece. *Clean. Energy Syst.* **2023**, *4*, 100055. [CrossRef]
26. SolarPACES. Partanna Ms-Lfr Csp Project. 2022. Available online: https://solarpaces.nrel.gov/project/partanna-ms-lfr (accessed on 30 July 2023).
27. Falchetta, M.; Mazzei, D.; Russo, V.; Campanella, V.A.; Floridia, V.; Schiavo, B.; Venezia, L.; Brunatto, C.; Orlando, R. The Partanna Project: A First of a Kind Plant Based on Molten Salts in Lfr Collectors. *AIP Conf. Proc.* **2020**, *2303*, 040001.
28. Falchetta, M.; Gambarotta, A.; Vaja, I.; Cucumo, M.; Manfredi, C. *Modelling and Simulation of the Thermo and Fluid Dynamics of the "Archimede Project" Solar Power Station*; Renewable Energy Processes and Systems; National Technical University of Athens: Athens, Greece, 2006; pp. 1499–1506.
29. Vignolini, M. *A New Approach to Concentrating Solar Plant (CSP) by ENEA*; ENEA: Brussels, Belgium, 2009.
30. Ferri, R.; Cammi, A.; Mazzei, D. Molten Salt Mixture Properties in Relap5 Code for Thermodynamic Solar Applications. *Int. J. Therm. Sci.* **2008**, *47*, 1676–1687. [CrossRef]
31. ENEA. *Laboratorio Di Qualificazione Collettori E Sistemi Solari*; Technical Report n° RT.2015.COL183.1; ENEA: Brussels, Belgium, 2015.
32. Blanco, M.J.; Mutuberria, A.; Martinez, D. Experimental Validation of Tonatiuh Using the Plataforma Solar De Almería Secondary Concentrator Test Campaign Data. In Proceedings of the 16th Annual SolarPACES Symposium, Perpignan, France, 21–24 September 2010.
33. Bonanos, A.M.; Georgiou, M.C.; Stokos, K.G.; Papanicolas, C.N. Engineering Aspects and Thermal Performance of Molten Salt Transfer Lines in Solar Power Applications. *Appl. Therm. Eng.* **2019**, *154*, 294–301. [CrossRef]
34. Merchán, R.P.; Santos, M.J.; Medina, A.; Calvo Hernández, A. High Temperature Central Tower Plants for Concentrated Solar Power: 2021 Overview. *Renew. Sustain. Energy Rev.* **2022**, *155*, 111828. [CrossRef]
35. He, Y.-L.; Qiu, Y.; Wang, K.; Yuan, F.; Wang, W.-Q.; Li, M.-J.; Guo, J.-Q. Perspective of Concentrating Solar Power. *Energy* **2020**, *198*, 117373. [CrossRef]
36. Forristall, R. *Heat Transfer Analysis and Modeling of a Parabolic Trough Solar Receiver Implemented in Engineering Equation Solver*; Technical Report, NREL/TP-550-34169; National Renewable Energy Laboratory: Golden, CO, USA, 2003.
37. Incropera, F.P.; Dewitt, D.P.; Bergman, T.L.; Lavine, A.S. *Fundamentals of Heat and Mass Transfer*, 6th ed.; Wiley: Hoboken, NJ, USA, 2012.
38. Crescenzi, T.; Mazzei, D. *Caratterizzazione Termica Tubi Ricevitori Schott*; ENEA Technical Report ENEA/SOL/RS/2005/15; ENEA: Brussels, Belgium, 2005.
39. Siemens. Star-Ccm+. 2021. Available online: https://www.plm.automation.siemens.com/global/en/products/simcenter/star-ccm.html (accessed on 30 July 2023).
40. European Commission. Photovoltaic Geographical Information System. 2022. Available online: https://re.jrc.ec.europa.eu/ (accessed on 30 July 2023).
41. Xiao, G.; Nie, J.; Xu, H.; Zhang, C.; Zhu, P. Performance Analysis of a Solar Power Tower Plant Integrated with Trough Collectors. *Appl. Therm. Eng.* **2022**, *214*, 118853. [CrossRef]
42. Kamel, S.; Agyekum, E.B.; Adebayo, T.S.; Taha, I.B.M.; Gyamfi, B.A.; Yaqoob, S.J. Comparative Analysis of Rankine Cycle Linear Fresnel Reflector and Solar Tower Plant Technologies: Techno-Economic Analysis for Ethiopia. *Sustainability* **2022**, *14*, 1677. [CrossRef]
43. SAM. System Advisor Model [Software], Version 21.11.2022. 2022. Available online: https://sam.nrel.gov/ (accessed on 30 July 2023).
44. Mohammadi, K.; Khanmohammadi, S.; Immonen, J.; Powell, K. Techno-Economic Analysis and Environmental Benefits of Solar Industrial Process Heating Based on Parabolic Trough Collectors. *Sustain. Energy Technol. Assess.* **2021**, *47*, 101412. [CrossRef]
45. Alsagri, A.S.; Chiasson, A.; Gadalla, M. Viability Assessment of a Concentrated Solar Power Tower with a Supercritical Co_2 Brayton Cycle Power Plant. *ASME J. Sol. Energy Eng.* **2019**, *141*, 051006. [CrossRef]
46. Khatti, S.S.; Jeter, S.; Al-Ansary, H. Preliminary Techno-Economic Optimization of 1.3 Mwe Particle Heating Receiver Based Csp Power Tower Plant for the Mena Region. In Proceedings of the ASME 2021 15th International Conference on Energy Sustainability, Virtual, Online, 16–18 June 2021.

47. Aseri, T.K.; Sharma, C.; Kandpal, T.C. A Techno-Economic Appraisal of Parabolic Trough Collector and Central Tower Receiver Based Solar Thermal Power Plants in India: Effect of Nominal Capacity and Hours of Thermal Energy Storage. *J. Energy Storage* **2022**, *48*, 103976. [CrossRef]
48. Aseri, T.K.; Sharma, C.; Kandpal, T.C. Estimation of Capital Costs and Techno-Economic Appraisal of Parabolic Trough Solar Collector and Solar Power Tower Based Csp Plants in India for Different Condenser Cooling Options. *Renew. Energy* **2021**, *178*, 344–362. [CrossRef]
49. Islam, M.T.; Huda, N.; Saidur, R. Current Energy Mix and Techno-Economic Analysis of Concentrating Solar Power (Csp) Technologies in Malaysia. *Renew. Energy* **2019**, *140*, 789–806. [CrossRef]
50. Arnaoutakis, G.E.; Katsaprakakis, D.A.; Christakis, D.G. Dynamic Modeling of Combined Concentrating Solar Tower and Parabolic Trough for Increased Day-to-Day Performance. *Appl. Energy* **2022**, *323*, 119450. [CrossRef]
51. Cheng, Z.-D.; Zhao, X.-R.; He, Y.-L.; Qiu, Y. A Novel Optical Optimization Model for Linear Fresnel Reflector Concentrators. *Renew. Energy* **2018**, *129*, 486–499. [CrossRef]